WATER RESOURCES RESEARCH, VOL. 49, 5355–5368, doi:10.1002/wrcr.20436, 2013

High-resolution distributed temperature sensing to detect seasonal groundwater discharge into Lake Væng, Denmark

E. Sebok,[1] C. Duque,[1,2] J. Kazmierczak,[1] P. Engesgaard,[1] B. Nilsson,[3] S. Karan,[1] and M. Frandsen[3,4]

Received 28 September 2012; revised 30 June 2013; accepted 17 July 2013; published 4 September 2013.

[1] Distributed temperature sensing (DTS) was used to map spatial and temporal changes in temperature on a 25 m by 6 m lakebed area in the winter (February), spring (May), and summer (August) of 2012. A constant and high discharge of groundwater with the average temperature of around 8°C to the lake will result in either lower (summer) or higher (winter) daily temperatures and reduce temperature variability at the sediment-water interface (SWI). DTS data were used as a proxy for groundwater discharge using three metrics; daily minimum temperature, diel amplitude, and daily standard deviation of temperature. During the seasons, the daily minimum temperatures at the SWI indicate a discharge zone 4–6 m offshore. From winter to summer, the extent of this zone changes and the SWI temperatures also show a shift of discharge locations toward the shore. Fluxes estimated on the basis of vertical temperature profiles from the top 50 cm of the lakebed and seepage meters in August compare well with the locations of the high-discharge zones detected by the DTS in the same period, giving confidence in the ability of the method to map both the areas and spatial variability of groundwater discharge to lakes. Compared to February, the DTS was able to detect new relatively cold temperature zones at the SWI in May and August indicating that groundwater discharge to the lake changes over time and that DTS can be used to monitor temporal variability in areas of discharge.

Citation: Sebok, E., C. Duque, J. Kazmierczak, P. Engesgaard, B. Nilsson, S. Karan, and M. Frandsen (2013), High-resolution distributed temperature sensing to detect seasonal groundwater discharge into Lake Væng, Denmark, *Water Resour. Res.*, *49*, 5355–5368, doi:10.1002/wrcr.20436.

1. Introduction

[2] The ecology of lakes is affected by internal and external fluxes of nutrients; internal fluxes being, for example, nutrients diffusively released from bottom sediments, while external fluxes are from sources outside the lake, such as inlets or groundwater discharge [*Shaw et al*., 1990]. Leaching of agricultural pollutants to groundwater in a lake catchment may therefore cause groundwater-dominated lakes to become eutrophic. Restoration is especially challenging for such eutrophic lakes, because it involves an assessment of where, when, and how much groundwater discharges to the lake.

[3] A characterization of groundwater-lake interaction at the scale of the lake involves a description of physiography, i.e., the setting of the lake in a catchment in terms of regional geology and landscape [*Winter*, 1981]. System geometries and parameters such as the ratio of the width of the lake to the thickness of the aquifer, slope of lake bed, regional aquifer heterogeneities, anisotropy in hydraulic conductivity, and how deep the lake penetrates the aquifer affect how a lake interacts with groundwater [*McBride and Pfannkuch*, 1975; *Pfannkuch and Winter*, 1984; *Winter and Pfannkuch*, 1984; *Cherkauer and Nader*, 1989; *Genereux and Bandopadhyay*, 2001]. In simple, homogeneous, and small aquifer-lake systems, the spatial distribution of discharge to a lake has been found to decrease exponentially with distance from the shore [*McBride and Pfannkuch*, 1975]. More commonly, heterogeneities in hydraulic conductivity play a significant role and can cause offshore peaks in groundwater discharge [*Cherkauer and Nader*, 1989; *Schneider et al*., 2005] and irregular patterns in discharge near the lakeshore [*Kishel and Gerla*, 2002; *Kidmose et al*., 2013]. Temporal variability in discharge makes groundwater-lake interactions even more complex. For example, rapid and large changes in discharge have been observed to be triggered by rainfall events [*Schneider et al*., 2005] leading to a sudden increase in the flux of nutrients from groundwater into lakes [*Downing and Peterka*, 1978].

[4] Accurate water and chemical budgets are needed when designing lake restoration schemes in order to assess the precise impact of a given measure. The groundwater component of a lake water budget is often evaluated as the residual of the water balance, estimated from flow net

[1]Department of Geosciences and Natural Resource Management, University of Copenhagen, Copenhagen, Denmark.
[2]Department of Geodynamics, University of Granada, Granada, Spain.
[3]Department of Hydrology, Geological Survey of Denmark and Greenland, Copenhagen, Denmark.
[4]Department of Biology, University of Copenhagen, Copenhagen, Denmark.

Corresponding author: E. Sebok, Department of Geosciences and Natural Resource Management, University of Copenhagen, Øster Voldgade 10, DK-1350 Copenhagen, Denmark. (Es@geo.ku.dk)

0043-1397/13/10.1002/wrcr.20436

approaches and isotopic tracers [*La Baugh et al*., 1997], or by integrating site-specific measurements (e.g., seepage meters) for the whole lake [*Shaw et al*., 1990]. This leads to uncertainty in the water and chemical budgets [*Shaw et al*., 1990] and sometimes to conflicting results [*La Baugh et al*., 1997]. It is therefore desirable to supplement existing methods with approaches that can map discharge zones at high resolution in both space and time so that well-designed field investigations can be carried out to obtain more accurate estimates of groundwater discharge into the lake.

[5] Groundwater discharge can be measured using different methods, for example, seepage meters have been often used to directly measure the vertical flux into a lake [*Lee*, 1977; *Schneider et al*., 2005; *Rosenberry et al*., 2010; *Kidmose et al*., 2011]. Heat as a tracer has also been successfully applied in many studies of groundwater-surface water interactions although mostly with respect to streams [*Anderson*, 2005; *Constantz*, 2008]. These heat-based studies have been used to not only locate discharge zones, but also to estimate the discharge flux from vertical streambed temperature profiles [*Schmidt et al*., 2007; *Jensen and Engesgaard*, 2011] or from time series analysis [*Hatch et al*., 2006; *Keery et al*., 2007]. There are a few examples from lakes where temperature profiles have been used to compare [*Kishel and Gerla*, 2002] or to estimate [*Kidmose et al*., 2013] vertical groundwater fluxes.

[6] Many of the existing methods only measure fluxes over a relatively small area, thus multiple measurements are needed to represent the spatial distribution of discharge to a section of a lake. Distributed temperature sensing (DTS) is a quick and noninvasive approach for mapping of temperatures at the sediment-water interface (SWI) [*Selker et al*., 2006a]. The fiber-optic cable of a DTS system is capable of measuring temperature with a resolution of up to 0.01°C and with a spatial-averaging interval of 0.25 m; detailed descriptions of the method are given in, for example, *Selker et al*. [2006a], *Tyler et al*. [2009], and *Suarez et al*. [2011].

[7] DTS has been widely applied to detect groundwater discharge to streams [*Selker et al*., 2006b; *Westhoff et al*., 2007; *Briggs et al*., 2011; *Krause et al*., 2012], wetlands [*Lowry et al*., 2007], and to study the thermal variations of saltmarsh channels [*Moffett et al*., 2008]. However, only a few studies have explored the use of DTS in lakes, for example, *Selker et al*. [2006a] recorded temperatures at the bottom of Lake Geneva across the almost 5 km wide lake and *Suarez et al*. [2011] studied the thermal evolution of the water column in an experimental solar pond.

[8] The use of DTS in lakes differs from stream applications in several ways. Due to the absence of stream flow, the installation of the cable in lakes is less complicated and for long-term measurements the effects of sedimentation and scouring are less prominent than can be the case in soft-bedded streams. A major challenge in lakes is the changing water depth in the littoral zone (where discharge typically occurs). The same discharge rate at a depth of 10 cm (near the shoreline) and 100 cm (further offshore) can result in two completely different temperature recordings due to the different effect of solar heating of the lake bottom. Due to this special environment that lakes represent for DTS applications, it is therefore necessary to study how external conditions such as solar heating affect the DTS temperature signals and their interpretation.

[9] Next to the mixing analysis [*Selker et al*., 2006b; *Westhoff et al*., 2007] usually carried out in DTS studies to quantify groundwater discharge, only *Briggs et al*. [2011] have compared DTS results in rivers with traditional methods like stream gauging and fluxes determined by geochemical mixing models and *Lowry et al*. [2007] used seepage meter measurements at three locations to verify concentrated groundwater discharge sites as detected by DTS. Nevertheless, to the knowledge of the authors the spatial variability in groundwater discharge indicated by DTS has never been compared to the spatial variability captured by traditional punctual measurements, for instance seepage meter measurements and fluxes estimated from vertical lakebed temperature profiles, methods widely used in lake studies to estimate groundwater fluxes. As the focus of previous DTS lake studies was not on detecting possible groundwater discharge areas, our main motivation was to see if DTS can be used in lakes to confidently map spatial and temporal variations in temperature signals thereby indirectly recording similar variations in discharge. The objectives of this study therefore have been to; (1) explore the use of DTS in lakes by combining measurements at the SWI and at several depths in the water column, (2) perform high-resolution measurements at the SWI during three seasons (winter, spring, and summer) to map spatial and temporal changes in discharge zones, and (3) to compare discharge areas detected by DTS with other proxies for groundwater discharge. These proxies are; maps of (i) indirectly estimated discharge from vertical lakebed temperature profiles using solutions to a 1-D analytical heat transport equation, (ii) directly measured discharge from seepage meters, and (iii) ice thickness during winter seasons.

2. Field Site

[10] Lake Væng is located in the upper part of Gudenå River catchment in central Jutland, Denmark (Figure 1a). The topographic catchment area of the lake is 10.7 km^2, excluding the lake area of 0.16 km^2. The lake has mean and maximum water depths of 1.2 and 1.9 m, respectively [*Jeppesen et al*., 1998], and an average volume of 187.000 m^3.

[11] Lake Væng has the longest history of attempted lake restoration in Denmark. The main ecological problem is related to very high total phosphorous (TP) concentrations. TP concentrations in the lake water were recorded monthly from 2008 to 2009 and ranged between 36 and 196 μg TP L^{-1}. *Kidmose et al*. [2013] measured an average TP concentration of 162 μg L^{-1} in discharging groundwater sampled from shallow boreholes around the lake, indicating a correlation between lake water and groundwater concentrations.

[12] Precipitation, calculated by the Danish Meteorological Institute for a 10 km by 10 km grid cell including Lake Væng, averages 787 mm yr^{-1} over the period 2000–2010 [*Scharling*, 1999]. Lake Væng has three minor inlets in the northern part and one major outlet in the southern end. The total discharge from the inlets was measured in 2011/2012 as part of this study and ranged between 10.8 and 47.0 L s^{-1}. The discharge at the outlet was continuously

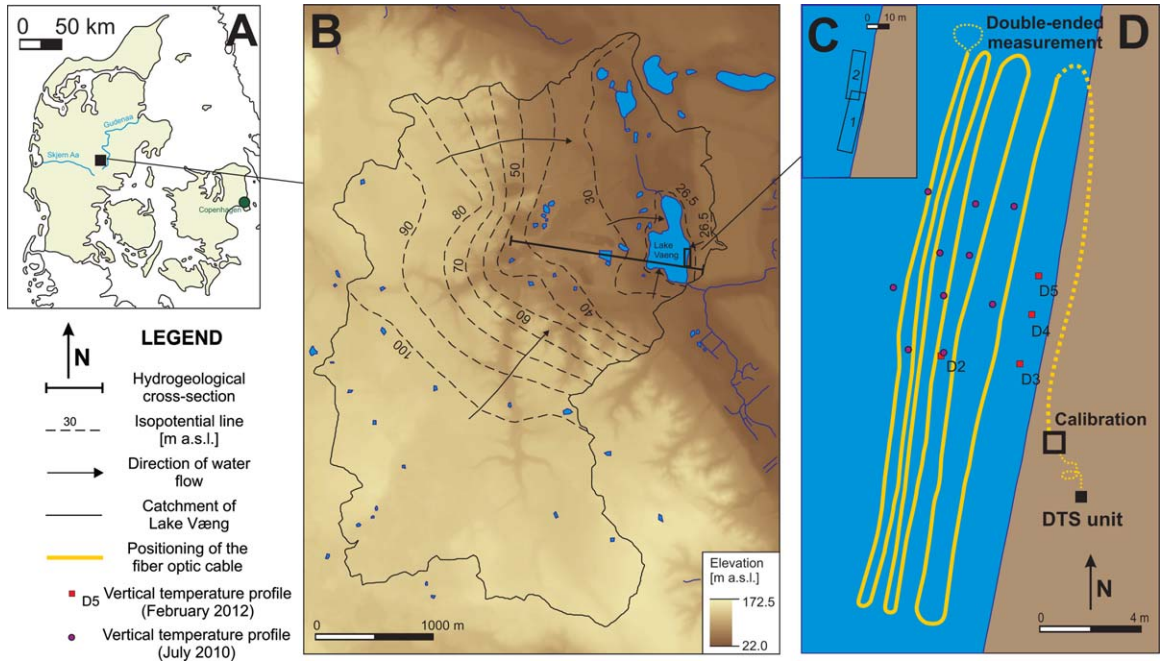

Figure 1. (a) Map of the study area showing the location of Lake Væng in Denmark and (b) its catchment with the topography and the isopotential map (both in meters above sea level) with directions of groundwater flow. (c) A map of the study area shows the location of the DTS temperature measurements at the SWI (1) and the location of multilevel water column measurements (2). (d) A sample layout of the SWI DTS loop from February 2012 and the locations of vertical temperature profiles from July 2010 and February 2012.

recorded from 2000 to 2008 and ranged between 135 and 165 L s^{-1} [*Nilsson et al*., 2010]. *Kidmose et al*. [2013] reported that groundwater represents 66%, the three surface inlets 30%, and precipitation 4%, respectively, of the total water input to Lake Væng in 2009. Hydraulic retention time in the lake was estimated to be approximately 20 days [*Kidmose et al*., 2013]; Lake Væng is thus a groundwater-dominated lake with upward groundwater fluxes everywhere in the study section on the eastern shore (see below).

[13] The lake is connected to an unconfined aquifer (Figure 2) consisting of medium to coarse sands and gravels of Pleistocene glacio-fluvial origin, deposited in a northwest, southeast trending erosional valley [*Geological Survey of Denmark and Greenland*, 2012]. The valley cuts through previously deposited Pleistocene clays and sands, Miocene sand-rich fluvial and coal-bearing deposits, and Miocene marine clay-rich deposits with insets of fine sand [*Rasmussen et al*., 2010]. The low-permeability deposits are not present as continuous layers and the Miocene and Pleistocene sand aquifers are hydraulically connected. The lower-lying parts of the Pleistocene valley, including the bottom of the lake, are topped by organic sediments of up to 9 m thickness [*Kidmose et al*., 2013].

[14] Groundwater in the catchment flows mainly from west-southwest to east-northeast (Figure 1b). Groundwater levels range between ∼110 m above sea level (m.a.s.l) in the southern part of the catchment and ∼26.4 m.a.s.l at Lake Væng. The lake surface only changed a few centimeters in 2011/2012.

[15] The eastern shoreline of this lake was chosen as the location of this study, because seepage meter measurements and 2-D groundwater flow modeling by *Kidmose et al*. [2013] showed that discharge at this shore can vary in space by as much as a factor of 50. Moreover, discharge

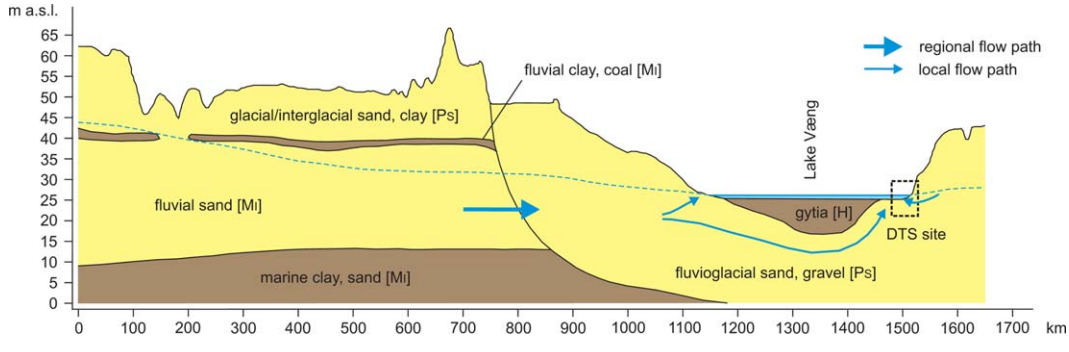

Figure 2. Geological W-E cross section of the study area, see Figure 1b for location.

Table 1. Measurements Taken at the Field Site

Type of Measurement	Time of Measurements	Number of Measurement	Mean Flux (m d^{-1})	Minimum Flux (m d^{-1})	Maximum Flux (m d^{-1})
DTS at the SWI	Feb 2012 May 2012 Aug 2012				
Multilevel lake water DTS	May 2012				
Temperature profiling	Jul 2010	10	0.14	0.03	0.21
	Feb 2012	4[a]	1.21	0.35	3.46
	Aug 2012	65	0.16	0.06	0.35
Seepage meter	Jan 2010	4[b]	2.07	0.2	6.3
	Aug 2012	39[c]	0.15	0.0027	0.62
Ice thickness	Feb 2010 Feb 2012	244			

[a]Measurements at ice hole and ice free locations.
[b]Measurements at ice hole locations.
[c]Triplicate measurements.

may even increase exponentially with distance from the shoreline, opposite to what is usually observed. This is due to organic sediments at the bottom of the lake creating a flow barrier [*Kidmose et al*., 2013], thus part of the groundwater flowing from west bypasses the lake and discharges near the eastern shore (Figure 2). In addition, there is a water table divide east of the lake resulting in a small groundwater contribution from this side (Figures 1b and 2).

3. Methods

[16] Distributed Temperature Sensing was used to locate areas of groundwater discharge in the littoral zone of the eastern shoreline (Figures 1d and 2). These temperature observations were compared with other methods used to estimate groundwater discharge; vertical temperature profiles in the upper 0.5 m of the lakebed to indirectly estimate fluxes, seepage meter measurements to directly measure groundwater discharge, and ice thickness measurements as a proxy for high groundwater discharge areas. Table 1 summarizes the different measurements carried out at the study site.

3.1. Distributed Temperature Sensing

[17] DTS was applied in two ways; (1) in a looped layout at the SWI covering a horizontal area of approximately 25 m by 6 m (Figures 1c and 1d) and (2) in a looped layout in the water column covering a volume of the lake of 21 m by 2 m by 0.6 m slightly north of the area used for the DTS on the SWI (Figures 1c and 3). The spatial extent of the DTS study section at the SWI was largely determined by the ice thickness observations of February 2010 and 2012 (section 3.4). The two DTS sites did not overlap in order to minimize sediment disturbance.

3.1.1. DTS: Temperature Measurements at the SWI

[18] A Damsense fiber-optic cable attached to a Sensornet DTS system (Oryx DTS-SR) was deployed on the lakebed between 17–19 February, 21–22 May, and 3–5 August 2012 to map groundwater discharge zones at different times of the year with different contrasts in temperature between lake water and groundwater. However, in the analysis complete 24 h data sets from 0.00 A.M. to 12 P.M. on 18 February, from 11.30 A.M. on 21 May to 11.30 A.M. on 22 May, and from 0.00 A.M. to 12 P.M. on 4 August 2012 are compared. In the double-ended measurements, the spatial averaging interval was 1.01 m along the cable with 0.12°C precision, integrated over 20 min. The temperature offset calibration of the double-ended installations was carried out by having 30 m of fiber-optic cable in a calibration bath at the lakeshore (Figure 1d).

[19] The fiber-optic cable was fixed to the lakebed in a looped layout with iron staples (Figure 1d) and deployed at the same study section during the three campaigns, however the individual layouts were slightly different. Each setup contained 6–8 unevenly spaced cable rows with an average of 0.5 m separating the rows further offshore and approximately 1 m spacing closer to the shore. Due to emergent vegetation no temperature measurements were taken directly at the shoreline. The DTS layout thus recorded an average temperature approximately at each meter along the 25 m study section and every 0.5–1 m cross shore.

[20] Temperature data were analyzed on the basis of three metrics; the diel amplitude (difference between daily

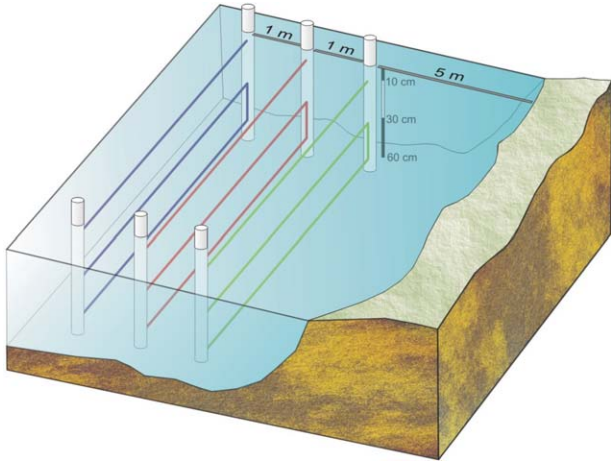

Figure 3. The layout of the DTS cable for the multilevel lake water temperature measurements. The location is shown in Figure 1d.

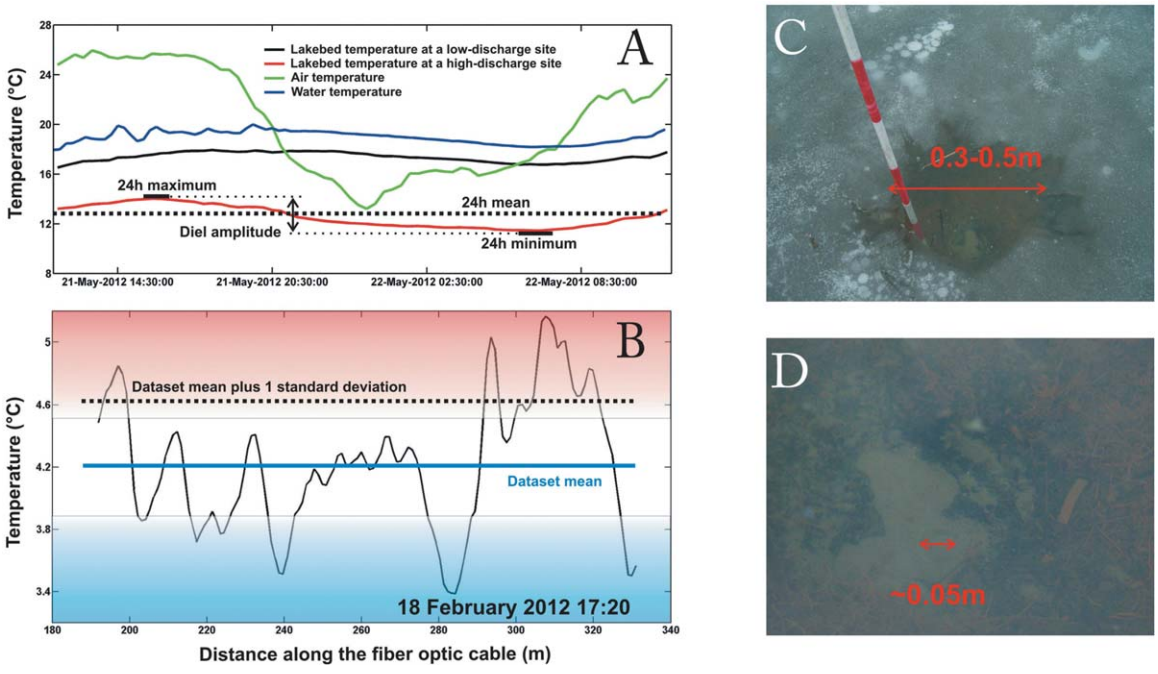

Figure 4. (a) The calculation of the daily mean, minimum, maximum temperatures, and the diel amplitude at a measurement location for a 24 h period in May. Note that the low-discharge site has a lower diel amplitude than the high-discharge site. (b) The special coloring scheme applied to the variables to emphasize anomalies is presented on the February 2012 data set where the measured daily minimum temperatures at each location along the fiber-optic cable are shown. The value for delineating the discharge areas (dashed line) was calculated by adding to the spatial mean of daily minimum temperatures (shown by the blue line) the standard deviation of this data set. This value was plotted as a contour line on the interpolated temperature map (Figure 5a) and used to separate possible high-discharge zones from low-discharge zones. (c) Ice hole of 0.3–0.5 m in diameter with the sand rings in motion (d) under the ice cover.

minimum and maximum temperatures), the daily standard deviation, and the daily minimum temperature (Figure 4a). Deeper groundwater in Denmark has an average temperature around 8°C; therefore high-discharge zones should show relative warmer areas at the SWI in the winter time and vice versa in the summer time. Furthermore, if discharge is stable then the changes in temperature at the SWI are reduced by the constant input of heat from groundwater. In other words, the diel amplitude or daily standard deviation of temperature should be lower in these areas. Spatial variability in groundwater discharge was visualized using interpolated maps of the metrics. A special coloring scheme was applied to emphasize the deviations from the spatial mean of the data set (Figure 4b).

[21] The discharge areas were delineated by taking the spatial mean of the daily minimum temperatures at the SWI plus one standard deviation of the daily minimum temperatures (February, shown in Figure 4b) or minus one standard deviation of the daily minimum temperatures (May and August). Discharge zones were named after the month they were detected and indexed based on their location in the study area (e.g., F_W is discharge in the Western zone in February).

3.1.2. DTS: Multilevel Lake Water Temperature Measurements

[22] The same type of DTS system and fiber-optic cable was fixed in a vertical looped layout (Figure 3) to the north of the SWI temperature measurements (Figure 1c). This setup allowed detection of any temperature stratifications or other variations arising from water circulation and enabled us to determine if temperature differences measured by the DTS at the SWI could be caused by changes in lake water temperature. The multilevel DTS system recorded temperatures between 22 and 24 May 2012 with a spatial-averaging interval of 1.01 m along the cable with 5 min integration times and 0.14°C precision at 0.1, 0.3, and 0.6 m depth from the lake surface. The cable was placed 5, 6, and 7 m from the shore at these three different depth levels. The analysis of the data was carried out with the same metrics as the DTS temperature data from the SWI.

3.2. Temperature Profiling

[23] Vertical groundwater fluxes were calculated indirectly by fitting an analytical solution to measured vertical lakebed temperature profiles recorded at the SWI study area at 10 locations in July 2010, four locations in February 2012 (just prior to the first DTS campaign), and 65 locations in August 2012 (immediately after the final DTS campaign). Thus, there was no data collection in the study section in between DTS campaigns in order to minimize disturbance of the lakebed.

[24] The probes were installed by the direct push method. In each profile, the temperature sensors were placed at 0, 0.025, 0.05, 0.075, 0.1, 0.15, 0.2, 0.3, 0.4, and

Table 2. Parameters Used in the Steady State Analytical Solution

Parameter	Symbol	Unit	Value
Density of the fluid	ρ_f	kg m^{-3}	999.73
Specific heat capacity of the fluid	c_f	J kg^{-1} °C^{-1}	4192
Effective thermal conductivity	κ_e	J m^{-1} s^{-1} °C^{-1}	1.84
Groundwater temperature	T_g	°C	8
Depth of constant groundwater temperature	L	m	5

0.5 m depths from the lakebed. The sensors were made of thermocouples that can measure with an accuracy of 0.2°C.

[25] *Bredehoeft and Papadopulos* [1965] gave the steady state analytical solution to the one-dimensional conduction-convection equation often used to interpret temperature profiles [*Schmidt et al.*, 2007; *Jensen and Engesgaard*, 2011];

$$T(z) = T_s + (T_g - T_s)\frac{\exp[N_{pe}z/L - 1]}{\exp(N_{pe} - 1)} \quad (1)$$

where T_s is the surface water temperature (°C), T_g is the temperature of the groundwater (°C) at a given depth L (m), z is the depth (m), and N_{pe} is the Peclet number describing the ratio of convection to conduction:

$$N_{pe} = \frac{q_z \rho_f c_f L}{\kappa_e} \quad (2)$$

where q_z is the vertical fluid flux in m s^{-1}, $\rho_f c_f$ the volumetric heat capacity of the fluid (J m^{-3}°C^{-1}), and κ_e is the effective thermal conductivity (J m^{-1} s^{-1} °C^{-1}).

[26] Vertical fluxes were calculated by fitting the analytical solution (equation (1)) to the observed temperature data with the parameters given in Table 2. The values of the variables were chosen based on *Jensen and Engesgaard* [2011]. The estimated fluxes were insensitive to reasonable choices of the depth of constant groundwater temperature (L). In all cases, the instantaneous temperature measured at the lakebed by the upper thermocouple was used as the upper boundary condition.

3.3. Seepage Meter

[27] Vertical fluxes were measured by seepage meters [*Lee*, 1977] at the four ice hole locations in January 2010 and again in August 2012 at 39 locations after the final DTS campaign. The seepage meters had a diameter of 57.5 cm and heights of 10, 15, or 25 cm. The top of the seepage meter was installed 2–5 cm above the lakebed and a plastic bag was prefilled with approximately 0.5 L lake water. A Plexiglass or a plastic box was fitted above the bag connected to a valve to prevent velocity-head effects [*Rosenberry*, 2008]. Measurements typically lasted from 20 min up to 1–2 h and were repeated three times. The mean of triplicate seepage meter measurements at each location at the DTS study section is presented. The seepage meter data was corrected with a factor of 1.1 because of friction loss in the seepage meter [*Rosenberry*, 2008].

3.4. Ice Thickness Measurements

[28] Ice thickness data were used as a proxy for groundwater discharge with the assumption that high discharge of relatively warmer buoyant groundwater would decrease ice thickness or in some cases even prevent ice formation resulting in holes of 0.3–0.5 m diameter in the ice cover of the lake as observed in February 2010 and 2012 (Figure 4c). As an indicator of concentrated groundwater discharge, sand rings in motion of 0.05 m diameter (Figure 4d) were sometimes observed at the lake bottom under the ice holes.

[29] Ice thickness data were collected in the study section in February 2010 at 244 locations aligned in four transects each running 30 m perpendicular to the shoreline. In

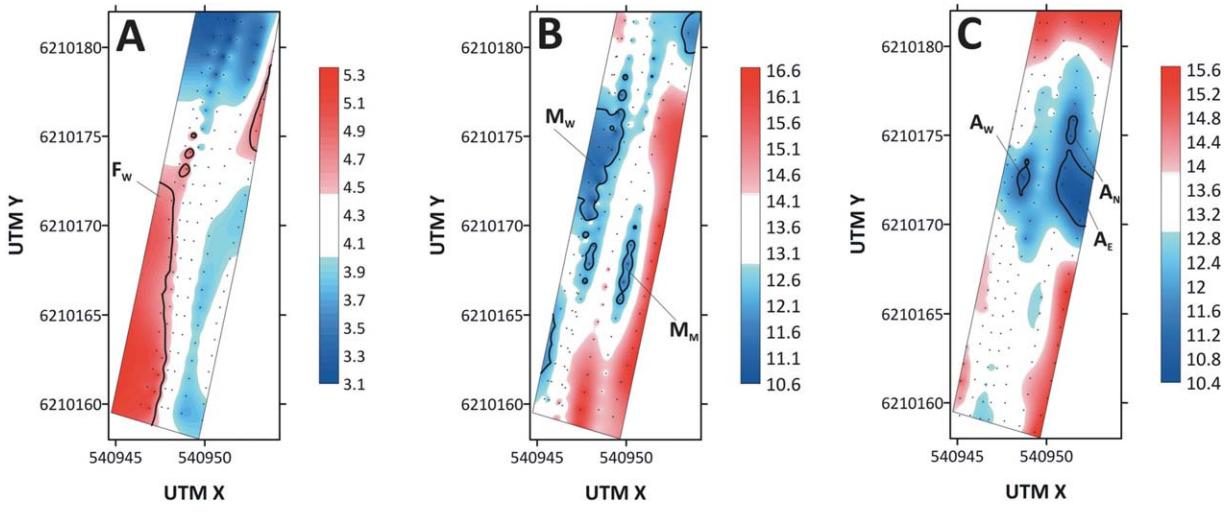

Figure 5. Daily minimum temperatures at the SWI in (a) February, (b) May, and (c) August 2012 with indication of the location of possible groundwater discharge zones. Temperature values are given in °C. The black dots denote the approximate DTS measurement points where an average temperature along 1.01 m of cable is collected. Measurements are available from different areas and interpolation was made for the whole area. Only the section where the common areas of the three DTS campaigns overlap with the other flux measurements is shown.

Table 3. Metrics for the February 2012, May 2012, and August 2012 Data Set[a]

	Data Set Location	Minimum Daily Temperature	Daily Standard Deviation	Diel Amplitude
Feb 2012	Western (F_W)	4.89	0.29	1.19
	Study site	4.19	0.46	1.64
May 2012	Western (M_W)	11.73	0.79	2.40
	Middle (M_M)	11.57	0.85	2.53
	Study site	13.54	0.72	2.26
Aug 2012	Western (A_W)	11.00	0.63	2.04
	Eastern (A_E)	10.90	0.72	2.21
	Northern (A_N)	10.98	0.63	1.96
	Study site	13.38	0.75	2.31

[a]All values represent a spatial mean and are given in °C.

February 2012, only the locations of the ice holes were marked before the removal of the ice cover and deployment of the fiber-optic cable on the lake bed (first DTS campaign).

4. Results

4.1. DTS

[30] The results are presented in terms of interpolated maps of temperature and daily variations in temperature (diel amplitude and daily standard variation). The daily minimum temperature maps represent the temperature observed at a specific location during a day. Although the whole data set is used for the interpolation, the interpolated maps only show the overlapping section of the three campaigns as the locations of the fiber-optic cable were different.

4.1.1. Temperature Measurements at the SWI

[31] Figure 5a shows the daily minimum temperatures at the SWI in February (recorded at 5 P.M.). The highest temperatures are observed in the Western (F_W) part of the study section compared with the spatial average of the whole data set (Table 3). The daily standard deviation (Figure 6a) and diel amplitudes (Figure 7a) in F_W are lower when compared with the spatial average of the data set as well. All three indicators of discharge (temperature at the SWI, diel amplitude, and daily standard deviation) suggest a spatial distribution of groundwater discharge, where the area at F_W is a high-discharge zone.

[32] In May, the DTS layout consisted of eight cable rows. Figure 5b shows the daily minimum temperatures (recorded at 5 A.M.). The lowest temperatures were observed at the Western (M_W) edge of the study section, where the minimum temperatures at the SWI are much lower compared to the spatial average of the data set (Table 3). A similar low-temperature zone can be detected closer to the shoreline in the middle of the section (M_M). This zone is new compared to February. These two areas (M_W and M_M) have average daily standard deviations (Figure 6b) and diel amplitudes (Figure 7b) slightly higher than the data set average (Table 3); thus contradicting the results based on the daily minimum temperatures.

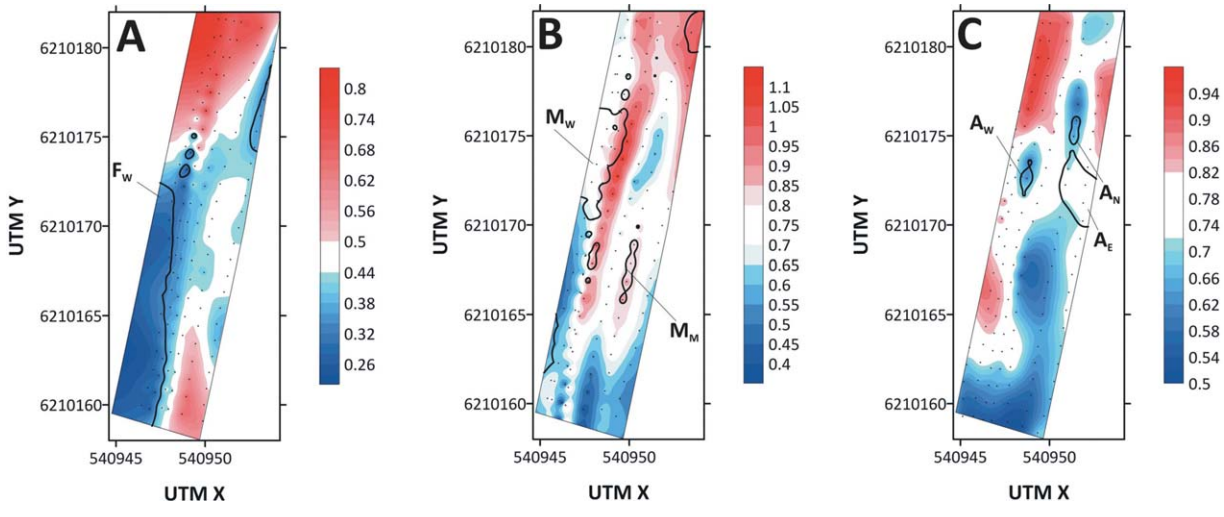

Figure 6. Daily standard deviation of temperature at the SWI in (a) February, (b) May, and (c) August 2012. Standard deviation values are given in °C. The solid black line indicates the areas where according to the daily minimum temperatures possible groundwater discharge zones are detected (Figure 5). The black dots denote the approximate DTS measurement points where an average temperature along 1.01 m of cable is collected. Measurements are available from different areas and interpolation was made for the whole area. Only the section where the common areas of the three DTS campaigns overlap with the other flux measurements is shown.

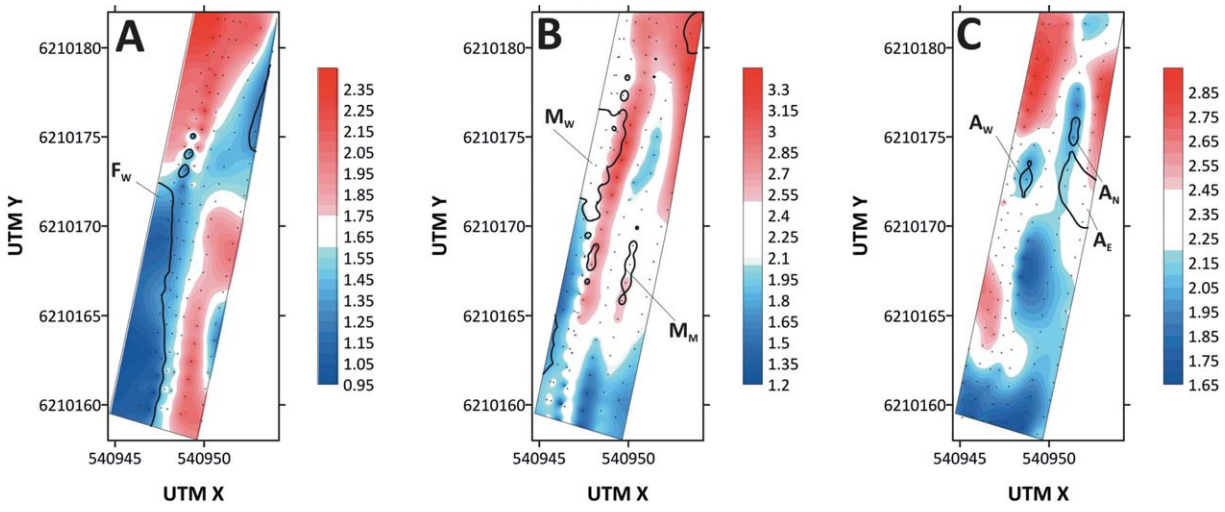

Figure 7. Diel amplitude of temperature at the SWI in (a) February, (b) May, and (c) August 2012. Diel amplitude values are given in °C. The solid black line indicates the areas where according to the daily minimum temperatures possible groundwater discharge zones are detected (Figure 5). The black dots denote the approximate DTS measurement points where an average temperature along 1.01 m of cable is collected. Measurements are available from different areas and interpolation was made for the whole area. Only the section where the common areas of the three DTS campaigns overlap with the other flux measurements is shown.

[33] In August, the DTS layout consisted of eight cable rows. Figure 5c shows the daily minimum temperatures recorded at 8 A.M. The results indicate small distinct cold areas at the Western (A_W) and Northern (A_N) end of the study section with a lower average minimum daily temperature compared to the whole data set (Table 3). However, the lowest minimum temperatures were observed in the Eastern end of the section (A_E) (Table 3), this area has now emerged as a new possible discharge zone. The average standard deviation and diel amplitude of the whole data set were higher than the standard deviation and diel amplitude observed in A_W and A_N, but only slightly higher than in A_E (Figures 6c and 7c and Table 3). All indicators agree on the location of A_W and A_N discharge zones, but the A_E zone is not confirmed by the daily standard deviation and diel amplitude.

4.1.2. Multilevel Lake Water Measurements

[34] Figure 8 shows the DTS results over 1.5 days in May. During this period, the air temperature varied by almost 13°C ranging from 13°C to 26°C (Figure 4a). During daytime, the DTS clearly detects a thermal layering in the water column. The water column warms up after sunrise, but with a time lag between the different depths. After sunset, the temperature distribution in the water

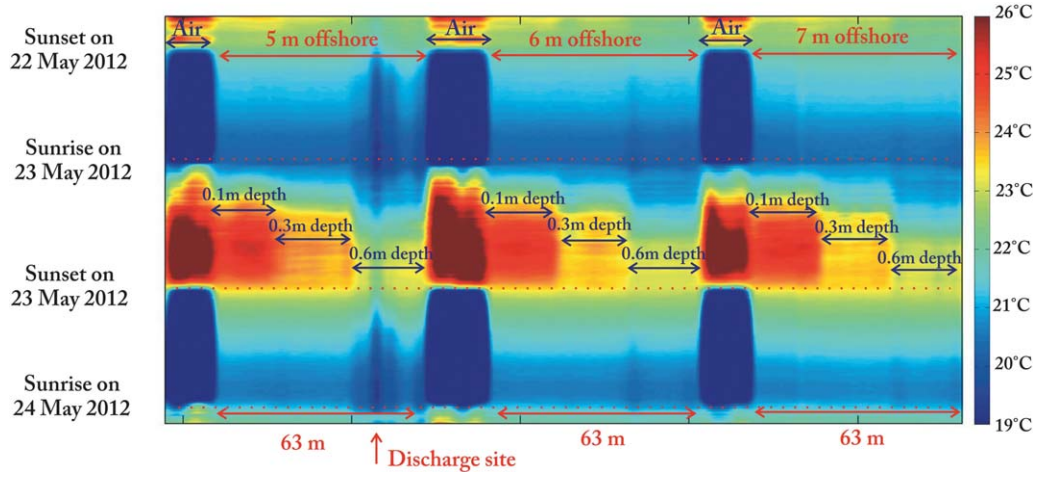

Figure 8. Water column temperatures measured along the cable with distances shown on the *x* axis and time on *y* axis. Distance is shown from the cable row located 5 m from the shoreline first at 0.1, then 0.3, and finally 0.6 m depth from the water surface, followed by the cable rows 6 and 7 m from the shoreline in a similar way (see also Figure 3). The sections in between these cable rows with the highly variable temperature are the sections of cable placed in the air.

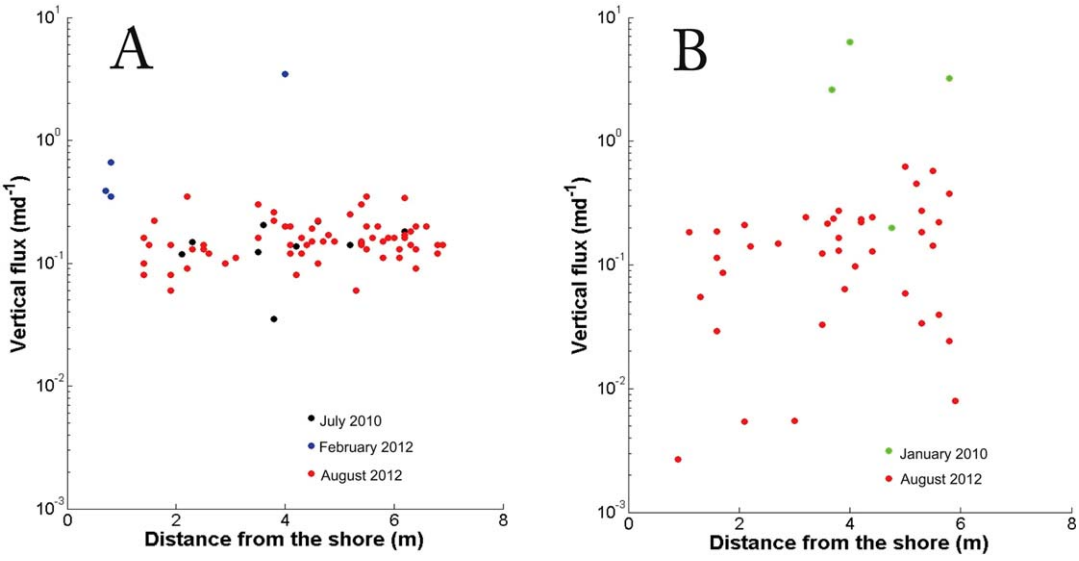

Figure 9. Vertical groundwater fluxes calculated on the basis of (a) vertical lakebed temperature profiles and (b) fluxes obtained by seepage meter measurements. Note the logarithmic scale on the *y* axis, fluxes increase upward.

column rapidly becomes homogeneous, but with a slow cooling off period. Figure 8 also shows a homogeneous water temperature distribution irrespective of depth at nighttime implying that the daily minimum SWI temperatures recorded during the night (and thus used in this study to detect discharge zones in May and August) are not influenced by solar radiation. The DTS detected a possible discharge site 5 m offshore (Figure 8) recording consistently low temperatures during the measurement period.

4.2. Heat Transport Modeling

[35] Vertical fluxes were first estimated on the basis of 10 vertical lakebed temperature profiles recorded in July 2010 (Figure 1d), 1.5 years before the first DTS campaign. The average flux is 0.14 m d^{-1} with a maximum flux of 0.21 m d^{-1} (Table 1).

[36] In February 2012, immediately prior to the first DTS campaign, three temperature profiles D3–5 (Figure 1d) were measured close to the lakeshore, while profile D2 was recorded in an ice hole (H3, see below), located in the middle of the DTS section. The highest flux of 3.46 m d^{-1}

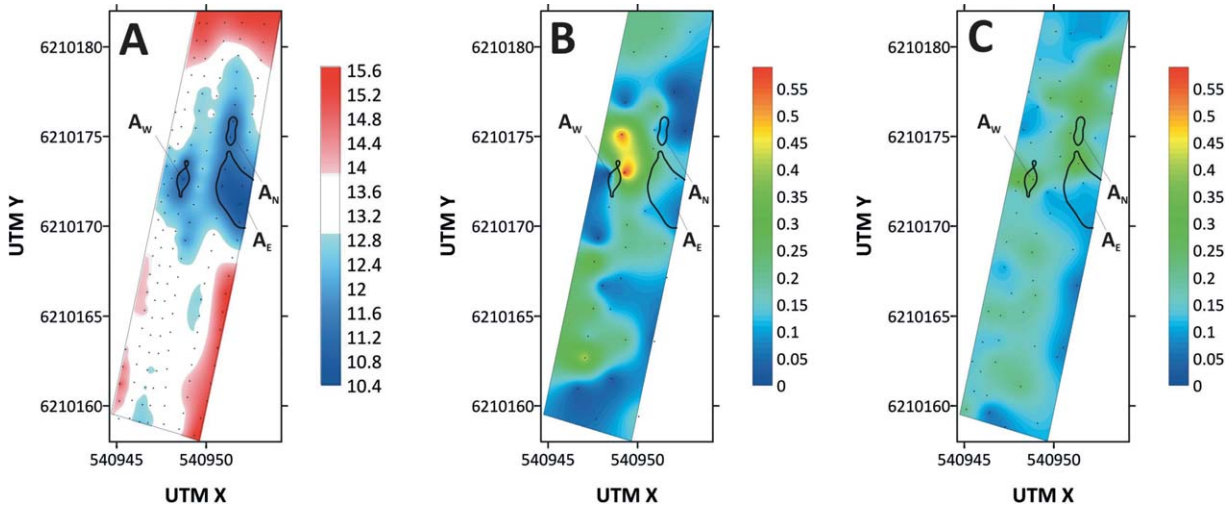

Figure 10. Contour maps of (a) the minimum temperatures at the SWI recorded by the DTS, (b) the vertical fluxes measured directly by seepage meters, and (c) the vertical fluxes calculated on the basis of temperature profiles during the August 2012 field campaign. Temperature values are given in °C and vertical fluxes in m d^{-1}. In Figure 10a, the black dots denote the approximate DTS measurement points where an average temperature of 1.01 m along cable is collected. In Figures 10b and 10c, the black dots show the location of the seepage meter or vertical temperature profile measurements, respectively. Measurements are available from different areas and interpolation was made for the whole area. Only the section where the common areas of the three DTS campaigns overlap with the other flux measurements is shown.

was measured at D2, with fluxes at the shoreline being an order of magnitude lower; 0.66 m d^{-1} at D3, 0.35 m d^{-1} at D4, and 0.39 m d^{-1} at D5.

[37] Figures 9a and 10c show the estimated fluxes in the study section in August 2012 (65 profiles). Observed fluxes ranged between 0.06 and 0.35 m d^{-1} and show great spatial heterogeneity (Table 1 and Figure 10c), the highest fluxes were recorded at the western and northeastern end of the study section (spatial mean of 0.31 m d^{-1}).

4.3. Seepage Meter

[38] In January 2010, seepage meter measurements in the ice holes showed fluxes of 0.2 m d^{-1} (HA), 6.3 m d^{-1} (HB), 3.2 m d^{-1} (HC), and 2.6 m d^{-1} (HD) (Table 1). Based on triplicate measurements at 39 locations, vertical fluxes in the DTS section ranged between 0.0027 and 0.62 m d^{-1} (Table 1 and Figure 9b) in August 2012. The maximum groundwater discharge of 0.62 m d^{-1} was measured at the western end of the study section (Figure 10b).

4.4. Ice Observations

[39] Figure 11 shows a map of the ice thickness and the location of ice holes as observed in February 2010 and in February 2012, 2 years later. The maximum ice thickness in the DTS section in 2010 was 0.16 m with four ice-free locations; ice holes HB, HC, and HD grouped together in the northern part of the study section with HA located in the southern end. The locations of HB and HC match the locations of H4 and H3 recorded in 2012 with a small change of approximately 0.1 m and 0.4 m. The HA and HD ice holes were not found again in 2012, instead two new ice holes had appeared (H1 and H2).

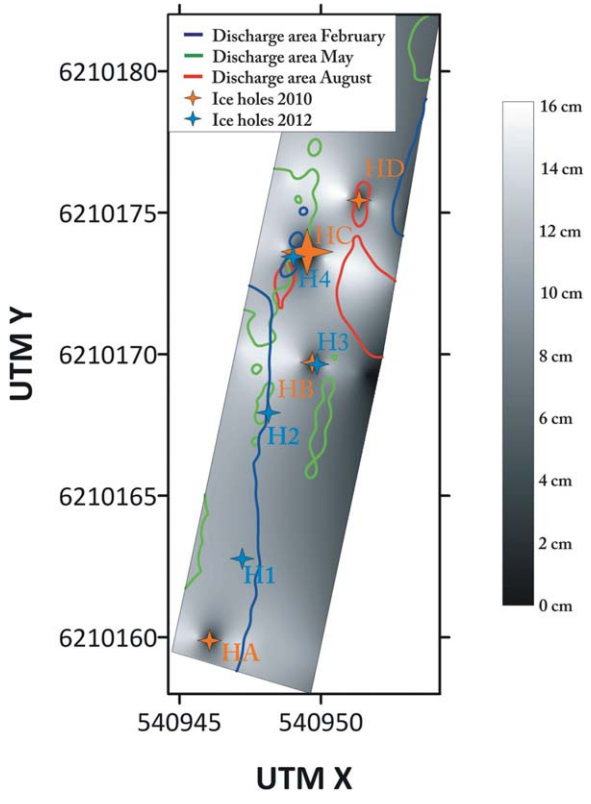

Figure 11. Contour map of the ice thickness from February 2010 with the observed location of the ice holes in February 2010 and 2012 and the delineated discharge zones for each study period. Measurements are available from different areas and interpolation was made for the whole area. Only the section where the common areas of the three DTS campaigns overlap with the other flux measurements is shown.

5. Discussion

[40] Compared to stream applications, the quasi-motionless water body of lakes represents a special environment for DTS applications. Due to the incoming shortwave radiation, the heating of the water column and the SWI is inevitable. However, for the DTS applications a more challenging problem is the heating of the fiber-optic cable which will record temperatures in excess of the bulk temperature of the SWI it is placed on, referred to as excess temperature [*Neilson et al*., 2010]. The excess temperature depends mainly on the intensity of solar radiation, water depth and turbidity, the color of the fiber-optic cable, and the lake bed substrate. *Neilson et al*. [2010] found that due to water flow and mixing of heat, solar radiation in a stream only resulted in an excess temperature of 0.01–0.17°C. Due to the decreased water velocity, the mixing of heat in the water column is less typical in lakes (Figure 8) thus the excess temperature can be higher and even more strongly related to water depth.

[41] As in this study the North-South oriented lakebed section only had topographical shading, it is assumed that lake water temperatures measured at the same depth are exposed to the same solar heating. Indeed, the DTS shows the influence of water depth and solar radiation on water temperature resulting in a gradual thermal layering during the sunshine hours and its rapid disappearance during the night (Figure 8). Thus, only night measurements can reliably detect groundwater discharge during periods with high solar radiation (to avoid uncertainties arising from excess temperatures).

[42] While in this study the effect of solar radiation is negligible in winter, this is not the case for the May and August campaigns. For the interpretation of the May and August data however, the daily minimum temperatures were used. These temperatures were recorded during the night when the multilevel lake water measurements revealed a relatively homogeneous temperature distribution in the water column (Figure 8), not showing the influence of solar radiation.

[43] However, both during the day and night measurements the multilevel lake water DTS detected significant groundwater discharge at one location at 0.6 m depth (Figure 8) showing the cooling effect of groundwater despite the solar radiation. During the winter, the positively buoyant groundwater prevents the formation of ice cover at a concentrated groundwater discharge site, therefore a dense layout of multilevel water column DTS together with DTS at the SWI could be applied to examine such three-dimensional thermal plumes.

[44] Lakebed temperature measured by DTS at the SWI as a proxy for groundwater discharge was evaluated using three metrics; (1) the minimum daily temperature, (2) the diel amplitude in temperature (maximum minus minimum

daily temperature), and (3) the daily standard deviation of temperature.

[45] The minimum temperature maps in February, May, and August (Figure 5) show high spatial variability indirectly reflecting a similar variability in discharge. The daily standard deviation and diel amplitude maps (Figures 6 and 7) also show great spatial and temporal variability, but also a distribution very similar to each other. In February, the lowest daily standard deviation and diel amplitude (Figures 6a and 7a and Table 3) match the discharge zones indicated by warm temperatures at the SWI (Figure 5a). Similarly, in August the minimum SWI temperatures at the A_W and A_N areas agree well with low daily standard deviations and diel amplitudes (Figures 5c, 6c, and 7c). There is however a disagreement between the three metrics in the case of M_W and M_M zones in May and the A_E zone in August. In May, the lowest temperatures were recorded in M_W and M_M, approx. 0.5 m apart from the area characterized by the highest daily standard deviations and diel amplitudes, while both the lowest daily standard deviations and lowest diel amplitude (Figures 6b and 7b and Table 3) were observed in the southern part of the area.

[46] The results in May can possibly be explained by a combination of the almost motionless shallow water and the high solar radiation due to warm and clear weather (Figure 4a). The cooling influence of groundwater discharge at the high-discharge locations resulted in generally lower SWI temperatures, although due to solar radiation these sites were also heated during the day. But after sunset, as opposed to low-discharge sites, the cooling effect of groundwater at high-discharge sites caused a more rapid and intense cooling (Figure 4a), leading to increased daily standard deviation values and diel amplitudes as shown in Figure 4a and quantified in Table 3.

[47] In August, in the A_W and A_N zones, the daily standard deviation and diel amplitude confirm the results of the minimum SWI temperatures. The difference in the agreement of the three metrics between May and August can possibly be due to differences in solar input. Although the lake water temperature is the same during the two campaigns, there are large differences in the air temperature and solar radiation. During May, clear skies and a gradual heating effect can be observed. In August, however, due to cloud cover, the air temperature was lower and fluctuated strongly after reaching a maximum at 10.00 A.M. Based on the air temperature data from both months, it is assumed that the warming effect of solar radiation was not enough to overcome the cooling effect of groundwater in August, thus all metrics detect groundwater discharge in the A_W and A_N zones.

[48] As decreased water velocity leads to less mixing of heat in lakes, a further challenge of DTS applications could be the entry of cold inlets or surface runoff to the lake. During the August field campaign, we noted seepage-face runoff from the riparian zone (groundwater), which might have affected the DTS results at the A_E zone. Although the daily minimum temperatures indicated a possible discharge zone here, the diel amplitude and daily standard deviation did not confirm these results. Moreover, neither the seepage meter-based fluxes nor the temperature-based fluxes showed high values in the area. One reason can be the propagation of the negatively buoyant cold water on the SWI from the surface runoff to the lake.

[49] These observations demonstrate the enhanced influence of external conditions on the DTS data recorded in lakes, also emphasizing the importance of using metrics with different temporal aspects to detect groundwater discharge. The daily standard deviation and diel amplitude both reflect daily temperature variations, including the effects of solar radiation. On the other hand, the daily minimum temperatures were measured during the night, free from solar input, thus considered more reliable in spring and summer conditions. Cold inlets entering the lake however, may greatly affect daily minimum temperatures and also slightly influence the daily standard deviation and diel amplitudes, thus a comprehensive interpretation of all metrics is necessary at all times. Next to the effect of solar radiation and cold inlets, future studies could possibly identify more factors influencing DTS applications in lakes.

[50] Comparing data collected in different seasons (and years) enables the observation of short and long-term temporal and spatial changes in groundwater discharge. The DTS is able to identify a significant high-discharge zone that is stable throughout the study period, i.e., F_W in February, A_W in August, and despite the disagreement of metrics possibly also M_W in May (Figure 5), which corresponds to the ice hole location HC/H4 observed both in 2010 and 2012 (Figure 11). This result agrees with the conclusion of the field experiments and modeling study of *Kidmose et al*. [2013] who found that discharge increases with distance from shoreline. This is likely because groundwater mainly originates from the Western side of the lake and discharges to the lake as soon as the layer of organic sediments in the lake ends (Figure 2).

[51] Spatial variations in groundwater discharge are also manifested in the appearance of new possible discharge zones in August (A_N) and most probably also in May (M_M). The location of the A_N zone matches the location of the HD ice hole found in 2010. The M_M zone could be related to the ice hole HB/H3 observed in February, with the assumption that by May this H3 discharge zone could have shifted slightly closer to the shoreline (approximately 0.5 m).

[52] However, during the different seasons a temporal trend in the spatial distribution of groundwater discharge can also be observed. From winter to summer, groundwater discharge locations shift slowly toward the lakeshore and are of smaller spatial extent (Figure 11). While in February rather the Southern part of the Western zone contributes to discharge, in May only the Northern part of the section (M_W) shows possible strong groundwater influence and by August the contributing zone (A_W) becomes spatially restricted. As the lake levels only changed a few centimeters in 2011/2012, one explanation of the temporal change in the distribution of discharge could be a decrease in the water table and thus the head gradient on the Western side of the lake from where groundwater is mainly derived.

[53] The high degree of spatial and temporal variability of discharge detected by the DTS was also confirmed by the traditional punctual measurements. The ice hole observations in 2010 and 2012 visually indicated the existence of a few scattered high-discharge zones in the study section, implying that discharge was heterogeneous and temporally variable. The seepage meter and temperature-based

fluxes in the same area from August 2012 confirm the high degree of spatial variability shown both by the ice holes and the DTS campaigns, with fluxes ranging from very low to close to 0.6 m d^{-1} in isolated zones (Figures 9 and 10).

[54] Even though both the seepage meter-based and temperature-based fluxes are associated with uncertainties in the measurements and in the calculation of vertical fluxes (installation, assumption of vertical flow), the two approaches give the same spatial mean in August 2012 (0.15–0.16 m d^{-1}). Furthermore, the fluxes estimated from temperature profiles in the same area in July 2010 gave a similar mean flux of 0.14 m d^{-1} (but with a much lower variability than in August 2012). Compared to the temperature-based fluxes, seepage meter measurements in August 2012 gave a much wider range of fluxes (Table 1). *Kidmose et al*. [2013] found that seepage meter fluxes could vary in space by as much as a factor of 50. Our measurements suggest that the spatial variability in groundwater discharge is even higher (Table 1) which agrees with the results of *Lee* [1977] who found a range of fluxes between 8.64 × 10^{-4} and 0.22 m d^{-1} around a lake and *Rosenberry et al*. [2010] also found fluxes between 0.019 and 1.37 m d^{-1} in undisturbed measurements along a lakeshore. The distribution of discharge as represented by Figures 9, 10b, and 10c could therefore be even more heterogeneous.

[55] These temperature- and seepage meter-based fluxes do not show the same high fluxes as measured in the ice holes in January 2010 and February 2012 (Table 3). Possible explanations could be: (i) the seepage meters and temperature probes were not exactly placed at the same location as the ice holes observed in February 2012; (ii) the zones with high discharge had moved between February and August or (iii) due to a decrease in head gradient on the Western side of the lake, groundwater discharge also decreased. However, the temperature profile D2 measured directly in ice hole H3 in February (one of the ice holes present in both 2010 and 2012) gave a flux of 3.46 m d^{-1} very similar to the fluxes measured by seepage meters in January 2010.

[56] In August 2012, the spatial distribution of discharge detected by DTS and the traditional punctual methods could also be compared. Only the seepage meter-based fluxes agreed with the DTS data at the location of the A_W discharge zone (Figure 10b), where in the proximity of the potential discharge zone detected by the DTS, fluxes up to 0.62 m d^{-1} were observed. Temperature-based measurements show fluxes of 0.3 m d^{-1} in the A_N area (Figure 10c), which also coincides with the ice hole HD detected in 2010. Similarly in February, the DTS was only able to capture the H4 and H1 concentrated discharge zones, but not H2 and H3, although measurements from January 2010 and February 2012 confirmed fluxes up to 6.3 m d^{-1} at ice hole locations.

[57] Thus, the approximate location of all major discharge sites identified by the DTS was confirmed by seepage meter and temperature-based fluxes, but the DTS did not detect all the major discharge sites and did not reflect the complex spatial pattern that the traditional punctual measurements show. Contrary to our study, *Lowry et al*. [2007] could only confirm one out of two potential discharge sites detected by the DTS, where the groundwater spring was visible in the streambed sediments.

[58] These discrepancies between the DTS, flux measurements, and the ice holes as proxies for groundwater discharge can possibly be explained by either the magnitude of inflow that the DTS can detect or the spatial extent of the concentrated discharge sites. Based on the groundwater flux measurements of August, the DTS was capable of detecting fluxes larger than approximately 0.3 m d^{-1}. The spatial-averaging interval of the DTS installation used in this study was 1.01 m which can be compared to the size of the sand rings at the concentrated discharge sites (diameter of ∼0.05 m). The spatial extent of the concentrated discharge sites is considerably smaller than the spatial-averaging interval. Thus, it appears that small, but concentrated discharge sites may not be visible in the SWI temperatures averaged over 1.01 m, unless the fiber-optic cable is positioned directly on these sites and the contrast in temperatures is high. In stream applications, however, such concentrated discharge sites can be recorded with the gradual recovery in streambed temperatures detectable for several meters along a stream and cable. The spatial averaging of temperatures over 1.01 m distance in lakes may lead to even greater challenges in detecting concentrated discharge during the winter when positive buoyancy drives the warm groundwater away from the fiber-optic cable.

[59] Apart from a disturbance on the lakebed surface, the DTS method is still noninvasive compared to, e.g., seepage meter measurements; thus, it was also possible to preserve the original state of the field site. This way it was assured that the observed spatial variation in temperatures and indirectly in groundwater discharge is solely a result of changes in groundwater flow conditions and are not due to preferential flow paths created by the application of flux measurements methods modifying the deeper sediment structure. The installation of the cable is easy in lakes with gentle slopes, allows for more variation when deploying the fiber-optic cable, and the effects of sedimentation and scouring are small. Thus, within two days an area of 150 m^2 (25 by 6 m) was mapped with a single fiber-optic cable. The DTS method could therefore be a promising option for long-term monitoring of major discharge sites.

6. Conclusions

[60] Groundwater discharge zones were mapped at Lake Væng by measuring diurnal changes in temperatures at the sediment-water interface (SWI) using a looped DTS layout. Temperature data were evaluated by three different metrics; (1) the daily minimum temperature, (2) the diel amplitude, and (3) the daily standard deviation in temperature. DTS was used in three seasons; February, May, and August of 2012 and compared with other types of measurements or proxies for discharge; seepage meter- and temperature-based fluxes, and ice thickness measurements. Although the approximate location of major discharge sites detected by the DTS was confirmed by seepage meter and temperature-based fluxes, the DTS does not reflect the spatial variability in discharge detected by seepage meter and vertical temperature profile measurements. For example, the DTS is not able to show the same areas where ice holes were observed, which may be explained by not having the cable precisely overlaying these areas of reduced size.

[61] Nevertheless, the DTS was capable of detecting major discharge sites and showing not only a consistent

pattern having highest discharge in the most offshore western part of the study section, but also a shift of discharge areas toward the shoreline likely due to shifts in the head gradient. This is a result of the special groundwater-lake interaction, where groundwater originates primarily from the other side of the lake, flows underneath the lake, and discharges on the eastern side.

[62] Based on the results of this study, we observe the following: (i) DTS was able to capture spatial and temporal variations in temperatures at the SWI and could therefore be used in long-term installations to monitor groundwater discharge to lakes, (ii) DTS had difficulties detecting concentrated discharge zones of small size and spatial heterogeneity of fluxes, (iii) due to the quasi-motionless water body of the lakes, the influence of external conditions (solar radiation and cold inlets) on SWI temperatures are enhanced, (iv) thus several metrics of different temporal aspect are necessary for a comprehensive interpretation of the SWI temperature data, and (v) the method works best when the influence of solar heating is smallest, in the summer night measurements are required and the diel amplitude and daily standard deviation are not reliable metrics. The application of DTS with the layouts described in this work can represent a new methodology for studying lake-groundwater interactions in areas of greater spatial extent where temporal changes in discharge can occur.

[63] **Acknowledgments.** The authors would like to thank the students of a department field course for their valuable assistance with the field work in May. The study was supported by the Centre for Lake Restoration (CLEAR), the Centre for Hydrology (HOBE), both funded by the Villum Foundation and the Spanish Program for Postdoc Mobility of the Ministerio de Educacion. We are grateful to M. C. Westhoff, two anonymous reviewers, S. Krause, and J. Selker for their helpful comments which helped to improve the quality of the manuscript.

References

Anderson, M. P. (2005), Heat as a ground water tracer, *Ground Water*, *43*, 951–968.

Bredehoeft, J. D., and I. S. Papadopulos (1965), Rates of vertical groundwater movement estimated from the Earth's thermal profile, *Water Resour. Res.*, *1*(2), 325–328.

Briggs, M. A., L. K. Lautz, and J. M. McKenzie (2011), A comparison of fibre-optic distributed temperature sensing to traditional methods of evaluating groundwater inflow to streams, *Hydrol. Processes*, *25*, 1277–1290, doi:10.1002/hyp.8200.

Cherkauer, D. S., and D. C. Nader (1989), Distribution of groundwater seepage to large surface-water bodies—The effect of hydraulic heterogeneities, *J. Hydrol.*, *109*, 151–165.

Constantz, J. (2008), Heat as a tracer to determine streambed water exchanges, *Water Resour. Res.*, *44*, W00D10, doi:10.1029/2008WR006996.

Downing, J. A., and J. J. Peterka (1978), Relationship of rainfall and lake groundwater seepage, *Limnol. Oceanogr.*, *23*, 821–825.

Genereux, D., and I. Bandopadhyay (2001), Numerical investigation of lake seepage patterns: Effects of porous medium and lake bed properties, *J. Hydrol.*, *241*, 286–303.

Geological Survey of Denmark and Greenland (2012), Danish National Borehole Archive (Jupiter), Copenhagen. [Available at www.geus.dk.]

Hatch, C. E., A. T. Fisher, J. S. Revenaugh, J. Constanz, and C. Ruehl (2006), Quantifying surface water-groundwater interactions using time series analysis of streambed thermal records: Method development, *Water Resour. Res.*, *42*, W10410, doi:10.1029/2005WR004787.

Jensen, J. K., and P. Engesgaard (2011), Nonuniform groundwater discharge across a Streambed: Heat as a tracer, *Vadose Zone J.*, *10*, 98–109, doi:10.2136/vzj2010.0005.

Jeppesen, E., J. P. Jensen, M. Soendergaard, T. Lauridsen, P. H. Moeller, and K. Sandby (1998), Changes in nitrogen retention in shallow eutrophic lakes following a decline in density of cyprinids, *Arch. Hydrobiol.*, *142*(2), 129–151.

Keery, J., A. Binley, N. Crook, and J. W. N. Smith (2007), Temporal and spatial variability of groundwater-surface water fluxes: Development and application of an analytical method using temperature time series, *J. Hydrol.*, *336*, 1–17.

Kidmose, J., P. Engesgaard, B. Nilsson, T. Laier, and M. C. Looms (2011), Spatial distribution of seepage to a flow through lake: Lake Hampen, Western Denmark, *Vadose Zone J.*, *10*, 110–124.

Kidmose, J., B. Nilsson, P. Engesgaard, M. Frandsen, S. Karan, F. Landkildehus, M. Soendergaard, and E. Jeppesen (2013), Focused groundwater discharge to a eutrophic seepage lake: Implications for future lake restoration, *Hydrogeol. J.*, in press.

Kishel, H. F., and P. J. Gerla (2002), Characteristics of preferential flow and groundwater discharge to Shingobee Lake, Minnesota, USA, *Hydrol. Processes*, *16*, 1921–1934.

Krause, S., T. Blume, and N. J. Cassidy (2012), Investigating patterns and controls of groundwater up-welling in a lowland river by combining fibre-optic Distributed Temperature Sensing with observations of vertical hydraulic gradients, *Hydrol. Earth Syst. Sci.*, *16*, 1775–1792, doi:10.5194/hess-16–1775-2012.

La Baugh, J., T. Winter, D. Rosenberry, P. Schuster, M. Reddy, and G. Aiken (1997), Hydrological and chemical estimates of the water balance of a closed-basin lake in north central Minnesota, *Water Resour. Res.*, *33*(12), 2799–2812, doi:10.1029/97WR02427.

Lee, D. R. (1977), Device for measuring seepage flux in lakes and estuaries, *Limnol. Oceanogr.*, *22*, 140–177.

Lowry, C. S., J. F. Walker, R. J. Hunt, and M. P. Anderson (2007), Identifying spatial variability of groundwater discharge in a wetland stream using a distributed temperature sensor, *Water Resour. Res.*, *43*, W10408, doi:10.1029/2007WR006145.

McBride, M. S., and H. O. Pfannkuch (1975), The distribution of seepage within lakebeds, *J. Res. U.S. Geol. Surv.*, *3*(5), 505–512.

Moffett, K. B., S. W. Tyler, T. Torgersen, M. Menon, J. S. Selker, and S. M. Gorelick (2008), Processes controlling the thermal regime of salt-marsh channel beds, *Environ. Sci. Technol.*, *42*(3), 671–676.

Neilson, B. T., C. E. Hatch, H. Ban, and S. W. Tyler (2010), Solar radiative heating of fiber-optic cables used to monitor temperatures in water, *Water Resour. Res.*, *46*, W08540, doi:10.1029/2009WR008354.

Nilsson, B., P. Engesgaard, J. Kidmose, M. Frandsen, F. Landkildehus, E. Jeppesen, and M. Søndergaard (2010), Overvejelser om grundvandsindsivningen om Vængsø. En foreløbig undersøgelse [in Danish], Rapp. 2010/26, Geol. Surv. of Den. and Greenl, Copenhagen.

Pfannkuch, H. O., and T. C. Winter (1984), Effect of anisotropy and groundwater system geometry on seepage through lakebeds. 1. Analog and dimensional analysis, *J. Hydrol.*, *75*, 213–237.

Rasmussen, E. S., K. Dybklaer, and S. Piasecki (2010), Lithostratigraphy of the upper oligocene—Miocene succession of Denmark, *Geol. Surv. Den. Greenl. Bull.*, *22*, 1–92.

Rosenberry, D. O. (2008), A seepage meter designed for use in flowing water, *J. Hydrol.*, *359*, 118–130.

Rosenberry, D. O., L. Toran, and J. E. Nyquist (2010), Effect of surficial disturbance on exchange between groundwater and surface water in nearshore margins, *Water Resour. Res.*, *46*, W06518, doi:10.1029/2009WR008755.

Scharling, M. (1999), Climagrid—Denmark, Precipitation 10*10 km (vers. 2). Description of methods [in Danish], Tech. Rep. 99-15, Dan. Meteorol. Inst., Copenhagen. [Available at www.dmi.dk/dmi/tr99-15.pdf.]

Schmidt, C., B. Contant, M. Bayer-Raich, and M. Schirmer (2007), Evaluation and field-scale application of an analytical method to quantify groundwater discharge using mapped streambed temperatures, *J. Hydrol.*, *347*(3-4), 292–307.

Schneider, R. L., T. L. Negley, and C. Wafer (2005), Factors influencing groundwater seepage in a large, mesotrophic lake in New York, *J. Hydrol.*, *310*, 1–16.

Selker, J. S., L. Thévenaz, H. Huwald, A. Mallet, W. Luxemburg, N. van de Giesen, M. Stejskal, J. Zeman, M. Westhoff, and M. B. Parlange (2006a), Distributed fiber-optic temperature sensing for hydrologic systems, *Water Resour. Res.*, *42*, W12202, doi:10.1029/2006WR005326.

Selker, J. S., N. van de Giesen, M. Westhoff, W. Luxemburg, and M. B. Parlange (2006b), Fiber optics opens window on stream dynamics, *Geophys. Res. Lett.*, *33*, L24401, doi:10.1029/2006GL027979.

Shaw, R. D., J. F. H. Shaw, H. Fricker, and E. E. Prepas (1990), An integrated approach to quantify groundwater transport of phosphorous to Narrow Lake, Alberta, *Limnol. Oceanogr.*, *35*, 870–886.

Suarez, F., J. E. Aravena, M. B. Hausner, A. E. Childress, and S. W. Tyler (2011), Assessment of a vertical high-resolution distributed-temperature-sensing system in a shallow thermohaline environment, *Hydrol. Earth Syst. Sci.*, *15*, 1081–1093, doi:10.5194/hess-15-1081-2011.

Tyler, S. W., J. S. Selker, M. B. Hauser, C. E. Hatch, T. Torgersen, C. E. Thodal, and G. Schladow (2009), Environmental temperature sensing using Raman spectra DTS fiber-optic methods, *Water Resour. Res.*, *45*, W00D23, doi:10.1029/2008WR007052.

Westhoff, M. C., H. H. G. Savenije, W. M. J. Luxemburg, G. S. Stelling, N. C. van Giesen, J. S. Selker, L. Pfister, and S. Uhlenbrook (2007), A distributed stream temperature model using high resolution temperature observations, *Hydrol. Earth Syst. Sci.*, *11*, 1469–1480.

Winter T. C. (1981), Effects of water-table configuration on seepage through lakebeds, *Limnol. Oceanogr.*, *26*(5), 925–934.

Winter, T. C., and H. O. Pfannkuch (1984), Effect of anisotropy and groundwater system geometry on seepage through lakebeds. 2. Numerical simulation analysis, *J. Hydrol.*, *75*, 239–253.